IJMF, Iranian Journal of Materials Forming, Vol. 3, No. 2, pp 64-78
Printed in The Islamic Republic of Iran, 2016

New Geometry for TCP: Severe Plastic Deformation of Tubes

M. H. Farshidi*
Ferdowsi University of Mashhad, Mashhad, Iran

Abstract: Since tubes are widely used for different industrial applications, processing of tubes by the Severe Plastic Deformation (SPD) method has been the target of different attempts. Among these attempts, development of SPD processes for tubes based on Equal Channel Angular Pressing (ECAP) has been more successful. As an illustration, Tube Channel Pressing (TCP) has been presented as an attractive SPD process since a relatively homogenous strain can be imposed on different sizes of tubes by this process. However, since die/mandrel geometry has a remarkable effect on the deformation behavior of tube in this process, more efforts must be focused on the optimization of the geometry of this process. This work is aimed to examine a new die geometry for TCP in order to reduce the strain heterogeneity and rupture risk of tube through the process. For this purpose, the effects of different geometrical parameters on the deformation behavior of tube during the process are studied using FEM simulations. In these simulations, the rupture risk of tube is considered using a damage criterion and then, results of simulations are compared with experiments. Results show that the new geometry of TCP imposes more intense strain, causes less strain heterogeneity and results in less risk of rupture of tube during the process. In addition, comparison of simulations and experiments shows that the applied simulation method can predict the rupture of tube during TCP. Besides this, different geometrical parameters of the new geometry of TCP are optimized by simulations considering dimensions of tube.

Keywords: Severe plastic deformation, Tube, FEM simulation, Strain distribution, Rupture prediction

1. Introduction

During past decades, Severe Plastic Deformation (SPD) method has fascinated a remarkable attention due to its capabilities such as an impressive improvement of mechanical properties and an extensive grain refinement of materials. As an illustration, different SPD processes have been developed for SPD of elementary profiles such as sheets and rods. For Example, Equal Channel Angular Pressing (ECAP) [1], High Pressure Torsion (HPT) [2] and Accumulative Roll Bonding (ARB) [3] are well-known SPD processes developed till the start of the current decade [4]. Recently, notable attentions are given to SPD of more geometrically complicated profiles such as tubes. For instance, different attempts have been focused on development of SPD processes for tube based on ARB [5], HPT [6] and ECAP [7-13]. Among these attempts, development of SPD processes for tubes based on ECAP has been more successful and effective since this has less limitation for dimensions of tube, needs less complicated machinery device and imposes a relatively homogenous plastic strain in comparison of other processes. Therefore, different ECAP-based SPD processes for tubes have been developed such as tubular ECAP [7], Tube Channel Pressing (TCP) [8-9], Tubular Channel Angular Pressing (TCAP) [10] and Parallel Tubular Channel Angular Pressing (PTCAP) [11]. These processes are generally based on axisymmetric ECAP of tube wall by different geometries of dies and mandrels. As an illustration, TCP is defined as a process in which the tube wall is passed through a bottleneck region whereas multi-stage shear strains occur besides hoop strains as illustrated in Fig. 1 [8-9]. As shown before [9], each pass of TCP by conventional geometry

Received by the editors August 31, 2016; Revised October 8, 2016 and Accepted October 15, 2016.
*Corresponding author (farshidi@um.ac.ir)

causes imposing of an equivalent plastic strain of about 0.5-2 depending on the used geometrical parameters. This is comparable with other SPD process such as ECAP and ARB and therefore, TCP shall be classified as an SPD process [4, 9].

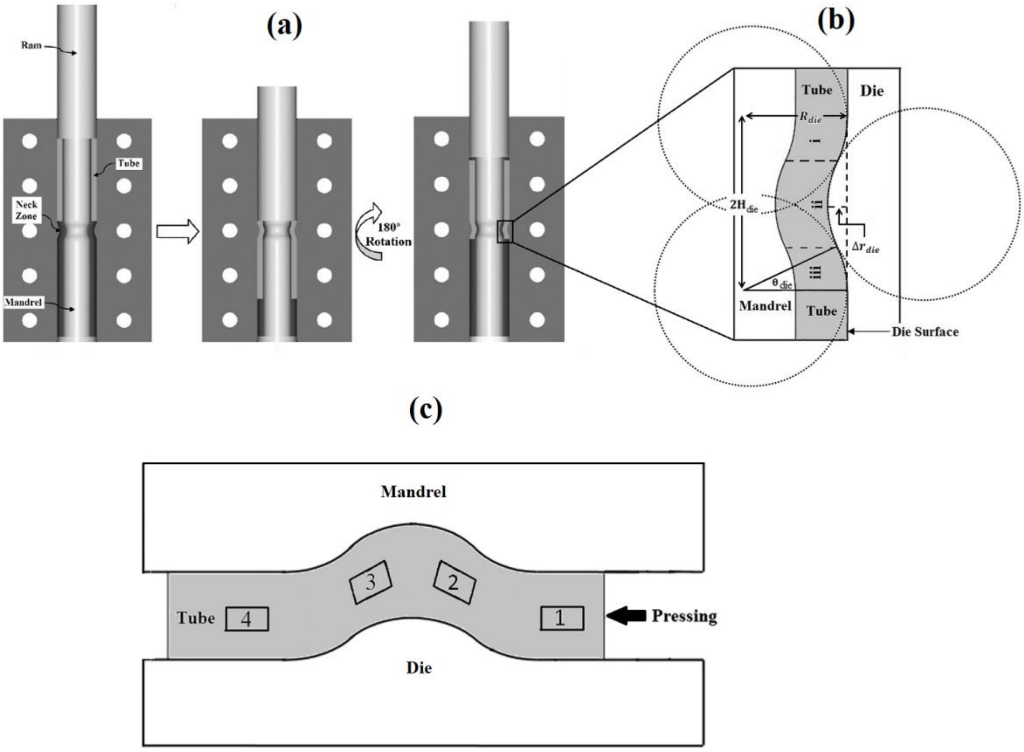

Fig. 1. (a) Schematic illustration and (b) geometrical parameters of the conventional TCP [9]. (c) Illustration of shear occurrence through TCP.

Although few studies have been focused on the effect of die/mandrel geometry on the deformation behavior of tubes through ECAP-based SPD processes, the effect of die/mandrel geometry on the rupture risk of tube through these processes have been remained less considered. In addition, previous studies have shown notable strain heterogeneity in these processes and previous attempts to reduce this strain heterogeneity were less successful. Besides this, previous works mainly discuss about general geometry of die/mandrel and they have paid little attention to detailed geometrical parameters of die/mandrel such as curvature radius [9-13].

The aim of this work is to investigate the distribution of strain, accumulation of damage and rupture of tube processed by a new geometry of TCP process. For this purpose, FEM simulations complemented by a damage criterion are applied to simulate accumulation of damage and rupture of aluminum 6061-O alloy through processing by different die/mandrel sets designed according to this new geometry. Besides this, rupture risk of the used tube through the process is experimentally practiced and compared with results of simulations to realize the validity of applied method for simulation of rupture risk of tube. This results in optimization of the new geometry of TCP to minimize both rupture risk and strain heterogeneity of tube through the process.

2. A new geometry of TCP

Figure 2a shows a schematic drawing of the new geometry of TCP and related parameters of its die and mandrel. As can be seen, the new geometry of TCP can be interpreted as four stages of shear strain accompanied by two stages of hoop strains on tube wall. In this new geometry, there is a distance between shear stages of TCP and the tube wall is flattening between these stages despite the conventional geometry. In addition, the curvature radius of die/mandrel in this geometry is smaller in comparison of the conventional geometry. The inner and outer diameters of tube are considered as 19 and 26 mm, respectively. As can be seen, variable parameters of the new geometry of TCP are as follows: the length of die convex (L_{die}), the length of mandrel cave ($L_{mandrel}$), the curvature radiuses of die and mandrel (R_{die} and $R_{mandrel}$), the channel angle ($\Theta_{channel}$), the height of die convex (Δr_{die}) and the depth of mandrel cave ($\Delta r_{mandrel}$). Considering previous studies, $\Theta_{channel}$ and Δr_{die} are considered as constant geometrical parameters for all die/mandrel sets and are valued as 150° and 1.5 mm, respectively [7-11]. In addition, the depth of mandrel cave ($\Delta r_{mandrel}$) is considered as 2.2 mm to save the area of cross section of tube in the middle of the bottleneck region to prohibit thinning of tube through TCP as long as be possible [12]. As shown before, the maximum imposed plastic strain accompanied by minimum deformation load through an ECAP process is obtained when the inner and outer curvature radiuses of its die are considered equal to each other [14-15]. Therefore, the R_{die} and $R_{mandrel}$ for new geometry of TCP are considered equal to each other. Regarding so, each die/mandrel set can be characterized by three exclusive geometrical parameters: L_{die}, $R_{die/mandrel}$ (R) and $L_{mandrel}$.

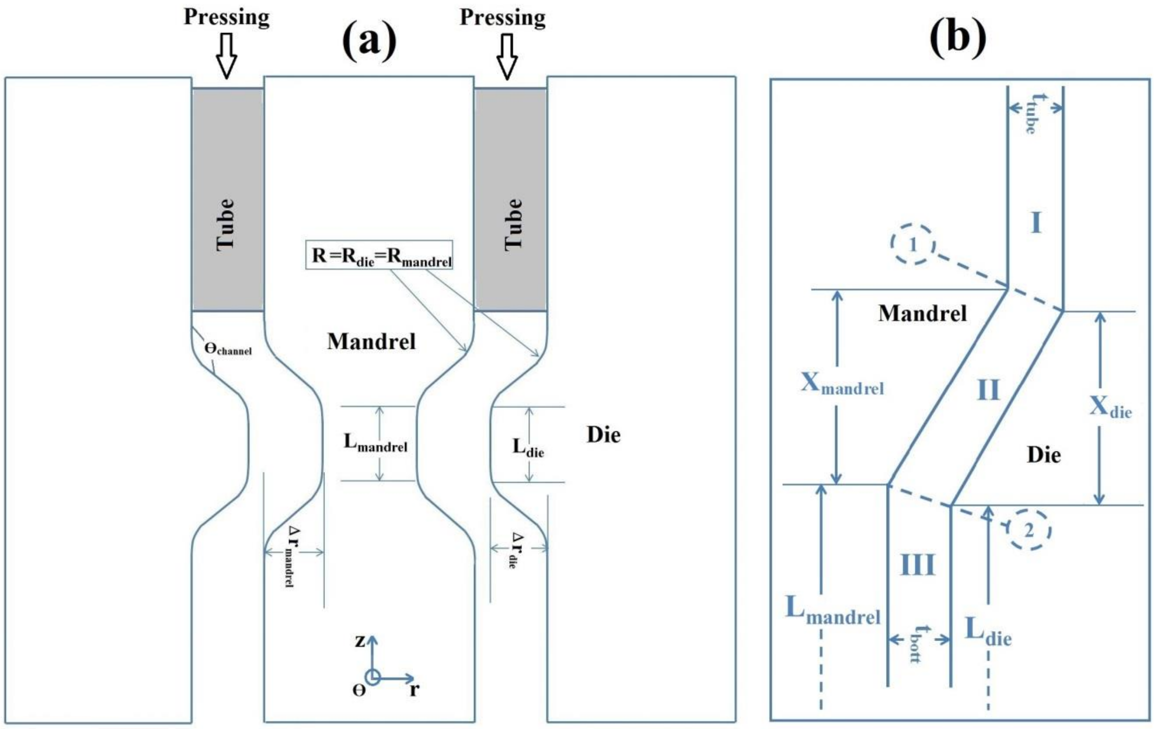

Fig. 2. (a) Schematic illustration of new geometry of TCP and related geometrical parameters.
(b) Illustration of two different scenarios for calculation of $L_{mandrel}$.

As illustrated before, selection of a great curvature radius for an ECAP-based SPD die causes increase of heterogeneity of imposed strain and appearance of multi-directional shear bands through the process [14-18]. In fact, the deformation mode changes from pure-shear to bending when a great curvature radius is selected for an ECAP die [15]. Therefore, this parameter shall not be selected too greater than the thickness of the specimen [14-15, 18-20]. However, there are different views about the optimum curvature radius and corner sharpness of ECAP dies [4, 15, 18-19]. As an illustration, previous works have shown that the increase of curvature radius of an ECAP die results in increase of strain heterogeneity while it may decrease the rupture risk of tube during the process [15,19]. Moreover, development of a new geometry for TCP needs more attention about curvature radius (R) since deformation behavior of a tube through TCP is relatively different from deformation behavior of a rod through the simple ECAP.

Considering these matters, four different amounts of 0.2, 1, 2.5, and 5 mm (≈ 0.06, 0.29, 0.71 and 1.42 times of tube thickness) are considered for curvature radius (R) of new geometry of TCP to evaluate the effect of this parameter on the deformation behavior of tube. Also, three different amounts from 0 to 10 mm are considered for L_{die} to realize the effect of this parameter.

As shown before [12], the thickness of tube in the middle of bottleneck region of a TCP die shall increase to save the cross section area of tube in order to prevent thinning of tube after the process. Therefore, Δr_{die} and $\Delta r_{mandrel}$ are different from each other and reasonably, L_{die} and $L_{mandrel}$ shall be also different. Consequently, two different scenarios can be considered for calculation of $L_{mandrel}$. In the first scenario, the $L_{mandrel}$ is calculated by considering the geometry of ECAP at first shear stage of TCP as presented in line 1 of Fig. 2b. In contrast, the second scenario considers the geometry of ECAP at second shear stage of TCP as presented in line 2 of Fig. 2b. Considering the first scenario, L_{die} and $L_{mandrel}$ can be related as below:

$$\frac{L_{mandrel}}{2} + \mathrm{X}_{\mathrm{mandrel}} = \frac{L_{die}}{2} + \mathrm{X}_{\mathrm{die}} + t_{tube}\, cot\, (\frac{\Theta_{\mathrm{channel}}}{2}) \tag{1}$$

where t_{tube} is the initial thickness of tube and X_{die} and $X_{mandrel}$ can be calculated as:

$$\mathrm{X}_{\mathrm{die}} = \Delta \mathrm{r}_{\mathrm{die}} \cot\, (\pi - \Theta_{\mathrm{channel}}) \tag{2}$$

$$\mathrm{X}_{\mathrm{mandrel}} = \Delta \mathrm{r}_{\mathrm{mandrel}} \cot\, (\pi - \Theta_{\mathrm{channel}}) \tag{3}$$

On the other hand, considering the second scenario, one may associate $L_{mandrel}$ to L_{die} as below:

$$\frac{L_{mandrel}}{2} = \frac{L_{die}}{2} + t_{bott}\, cot\, (\frac{\Theta_{\mathrm{channel}}}{2}) \tag{4}$$

where t_{bott} is the thickness of tube in the middle of bottleneck region which can be related to t_{tube} as below:

$$t_{bott} = t_{tube} + \Delta \mathrm{r}_{\mathrm{mandrel}} - \Delta \mathrm{r}_{\mathrm{die}} \tag{5}$$

Substituting different parameters of Eqs. (1) to (5) according to what mentioned in two previous paragraphs, it is clear that the first scenario considers $L_{mandrel}$ about 0.5 mm smaller than L_{die} while the second one calculates it about 2.2 mm greater than L_{die}. Thus, outputs of two different scenarios for calculation of $L_{mandrel}$ contradict each other. Regarding so, the optimization of geometry of TCP is divided in two steps: (a) optimization of L_{die} (b) optimization of $L_{mandrel}$ and R. During the first step, $L_{mandrel}$ is constantly considered as the average of two mentioned scenarios (about 0.9 mm greater than L_{die}) to investigate the effect of L_{die} on the deformation behavior of tube through TCP. Once this step is finished, the effect of $L_{mandrel}$ and R on deformation behavior of tube through TCP is investigated for optimization of these parameters. In this step, four different amounts of 0, 0.9, 1.9 and 2.9 mm are considered for $L_{mandrel}$.

3. Simulation and Validation Procedure

Deformation behaviors of aluminum 6061-O alloy tube through TCP process by different geometrical parameters are simulated by Abaqus 6.13 software using a 2D axisymmetric dynamic explicit FEM model based on Lagrangian formulation. The Lagrangian adaptive meshing method is applied on the specimen to decrease its mesh distortion through automatic aspect ratio improvement performed by software. Voce relation is used for extrapolation of flow stress vs. plastic strain curve since this relation can accurately predict this curve for aluminum alloys subjected to extensive plastic strain [21-22]. Die and mandrel are meshed by the CAX3 and CAX4R elements which respectively consist of 3 and 4 nodes. The mesh size for these parts is 7 mm for surfaces which have no contact with the specimen, 2 mm for surfaces which have contacts with specimen out of the bottleneck region and 0.5 mm for surfaces which have contact with specimen inside of the bottleneck region. The tube is meshed using 0.5×0.5 mm CAX4R elements. To investigate the mesh sensitivity of applied simulations, one simulation was carried out by halved sized meshes. Results of this simulation have shown a negligible difference in comparing the results of its typical size meshed counterpart. For example, the difference in the calculated equivalent plastic strain was less than 5%. The capabilities of the applied simulation procedure to predict both strain distribution and deformation load have been verified by experiments in previous works [9, 12].

Since extensive plastic strain is imposed during TCP process, the risk of rupture during this process should be considered. For this purpose, an accumulative damage criterion can be applied to evaluate the onset of rupture as below [22]:

$$\int_0^{\varepsilon_f} \frac{d\varepsilon_p}{\varepsilon_f(\eta)} = 1 \tag{6}$$

where $\varepsilon_f(\eta)$ is the rupture strain as a function of η, $d\varepsilon_p$ is the differential of plastic strain and η is the stress triaxiality defined as below:

$$\eta = \frac{\sigma_m}{\bar{\sigma}} \tag{7}$$

Here, σ_m is the average of normal stresses (negative of the hydrostatic pressure) and $\bar{\sigma}$ is the von-Misses equivalent stress. As shown before [22-24], the $\varepsilon_f(\eta)$ can be generalized as below:

$$\varepsilon_f(\eta) = \begin{cases} \frac{c_1}{1+3\eta} & -\frac{1}{3} < \eta < 0 \\ c_1 + (c_2 - c_1)\left(\frac{\eta}{\eta_0}\right)^2 & 0 < \eta < \eta_0 \\ c_2 \frac{\eta_0}{\eta} & \eta > \eta_0 \end{cases} \tag{8}$$

Here, η_0, c_1 and c_2 are material constants which have been respectively calculated as 0.39, 0.74 and 1.26 for aluminum 6061-O alloy by Kacem et al. [22].

To verify simulated occurrence of rupture by experiments, the aluminum 6061-O tube is processed by different passes of conventional TCP using strain rate of 0.01 S^{-1} and then, it is visually inspected to detect probable macroscopic cracks. Afterwards, the results of visual inspections of processed tube are compared by results of simulations for accumulated damage through TCP to realize the accuracy of applied simulation procedure for prediction of rupture.

4. Results and Discussion

Figure 3 shows the deformation behavior of tube using conventional geometry of TCP. As shown in Fig. 3a, the TCP processed tube can be divided to three different regions: an “unsteady-state” deformed region, a “steady-state deformed region” and a region “remained in bottleneck” after the process. At the beginning of process, the unsteady-state deformed region appears in which the tube wall can freely pass through the bottleneck zone with little frictional contact with die and mandrel surfaces which results in a limited hydrostatic pressure on tube during deformation. In addition, the amount of imposed strain is relatively low and distribution of strain is almost heterogeneous in this unsteady-state deformed region in comparison to its upper counterpart since the tube wall doesn’t correctly follow its route between die and mandrel. Therefore, the unsteady-state deformed region shall be considered as a wasted section. After the unsteady-state deformed region, the steady-state deformed region appears in which the tube wall is almost in full contact of die and mandrel surfaces during deformation which causes an impressive increase of deformation load and hydrostatic pressure on tube. In addition, a remarkable and relatively homogenous strain is imposed on tube wall in this region. The uppermost region is the one remained in bottleneck zone after the process and doesn’t completely complete the process. As can be seen, the imposed strain on this region is relatively low and therefore, this region shall be considered as a wasted section. It is also notable that since the next pass of TCP is imposed from the bottom of tube to upward, the unsteady-state deformed region and the remained region in bottleneck nearly replace each other in the next pass which means limited involvement of these regions in the process. Considering these explanations, it is clear that the only usable section of a TCPed tube is the steady-state deformed region whereas a considerable plastic strain is imposed almost homogeneously. Fig. 3b presents the distribution of normal stress in cylindrical direction of tube (σ_{zz}) through TCP process. As can be seen, the distribution of stress is almost smooth which implies the stability of simulation results. In addition, a remarkable residual stress after the TCP process can be observed in both sides of tube which is attributed to heterogeneity of strain distribution.

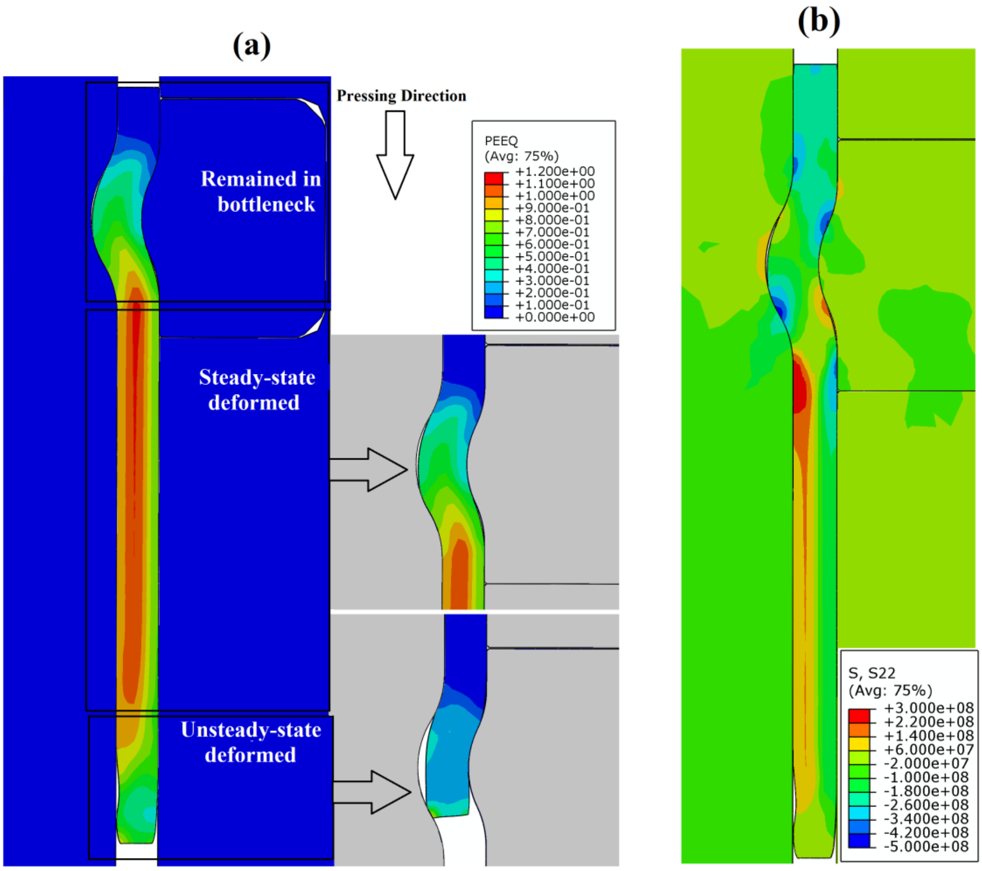

Fig. 3. Deformation behavior of tube using conventional geometry of TCP: (a) Distribution of imposed plastic strain and illustration of three differently deformed regions and (b) Distribution of normal stress in cylindrical direction (σ_{zz}) in tube during deformation.

Figure 4 compares the distribution of accumulated damage and rupture of tubes processed by one to four passes of TCP using the conventional geometry. As shown here, the accumulated damage on tube is more considerable in unsteady-state deformed region after one pass of TCP in comparison with other regions. This is due to imposing lower frictional pressure on this region through TCP as mentioned before. Nevertheless, the accumulated damages on uppermost and bottom of tube do not increase rapidly by imposing TCP passes since these regions are not completely involved in TCP as mentioned before. In addition, the amount of accumulated damage after one pass of TCP is significantly less than the criterion of 1 as shown in Fig. 4a which illustrates negligible risk of rupture. Correspondingly, no macroscopic crack is traced after one pass of TCP by experiments. As shown in Fig. 4b and c, the accumulated damage after two and three passes of TCP is also less than the criterion of 1 and comparatively, no macroscopic crack is experimentally observed after these passes. Despite this, the accumulated damage crosses the criterion of 1 after four passes of TCP, both in inner side and outer side of tube as shown in Fig. 4 (d). This implies probable occurrence of rupture in these areas of tube which is experimentally observed as illustrated in Fig. 4e and f. Comparing these results, it can be demonstrated that the applied simulation method can successfully predict the rupture of tube subjected to TCP.

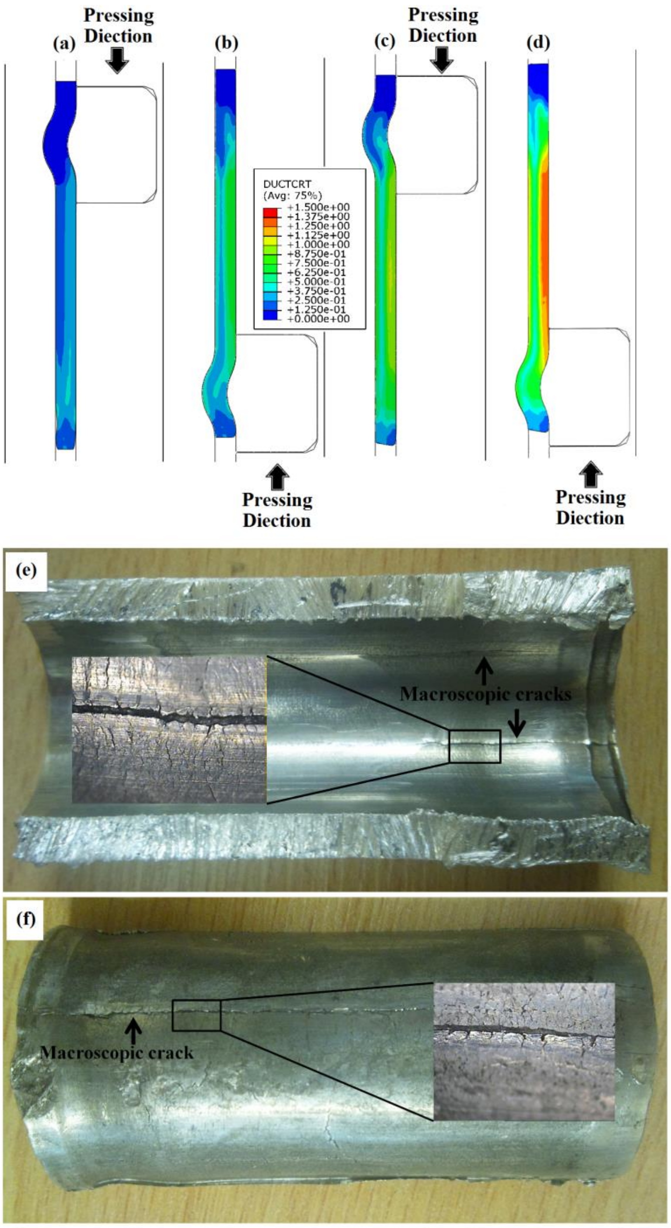

Fig. 4. Distribution of accumulated damage after: (a) 1 pass, (b) 2 passes, (c) 3 passes and (d) 4 passes of the conventional TCP. Rupture of tube after four passes of the conventional TCP: (e) inner side of tube and (f) outer side of tube.

Figure 5 compares the effect of L_{die} on the distribution of plastic strain in specimen processed using the new geometry of TCP. As can be seen, the length of the unsteady-state deformed region increases by increase of L_{die}. As an illustration, the die/mandrel sets designed by L_{die} of zero result in impressive smaller unsteady-state deformed regions. In addition, increase of L_{die} intensifies the damage accumulated in tube through the process as shown in Fig. 6. This is due to less hydrostatic pressure on tube during deformation caused by little frictional contacts between the tube and die/mandrel. When L_{die} is greater than 0 mm, the tube can freely pass through region III shown in Fig. 2b at initiation of the process which results in longer unsteady-state deformed region as well as less frictional contact between die/mandrel and tube. Besides this, increase of L_{die} results in increase of wasted material remained in the bottleneck zone after the process. Considering these explanations, it can be inferred that adoption of L_{die} equal to zero causes an impressive decrease in risk of rupture of tube and waste of material during the process. Therefore, the L_{die} has considered as 0 mm in forthcoming steps of this work.

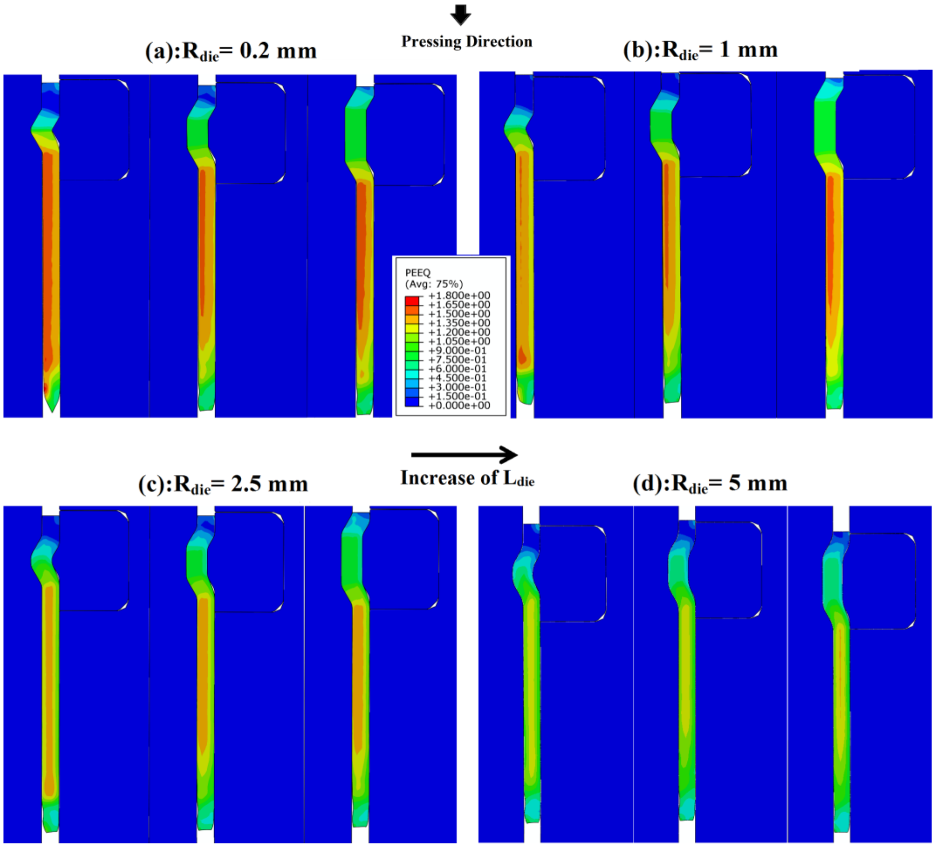

Fig. 5. The effect of L_{die} on distribution of equivalent plastic strain through TCP for die/mandrel sets designed by curvature radius (R) of: (a) 0.2 mm, (b) 1 mm, (c) 2.5 mm and (d) 5 mm.

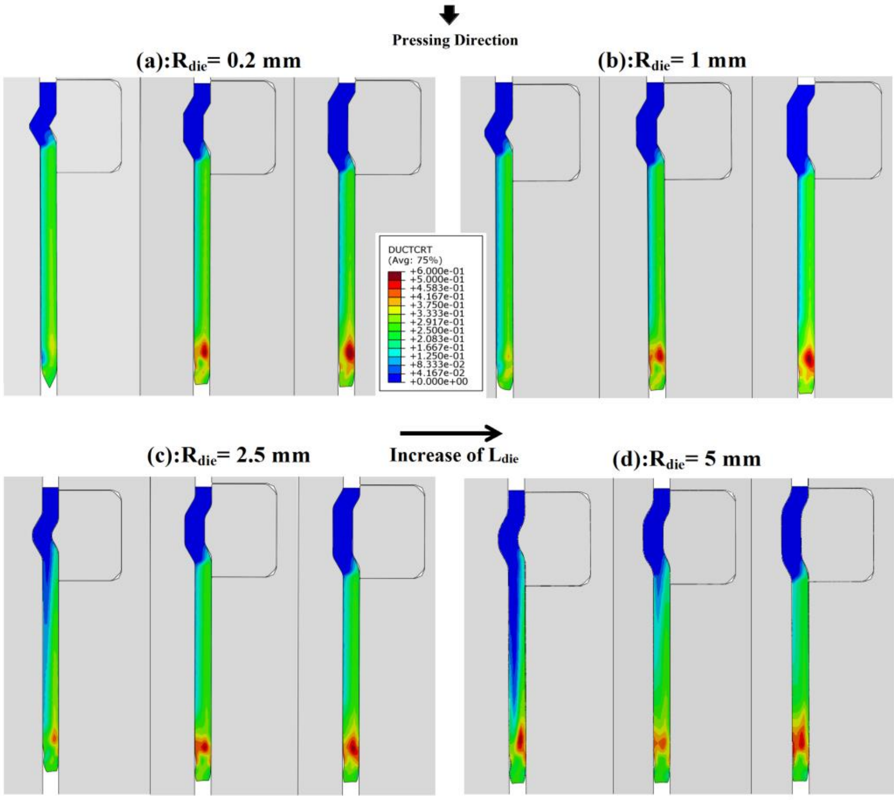

Fig. 6. The effect of L_{die} on accumulation of damage through TCP for die/mandrel sets designed by curvature radius (R) of: (a) 0.2 mm, (b) 1 mm, (c) 2.5 mm and (d) 5 mm.

Figure 7 compares the accumulated damage on tube through TCP using die/mandrel sets designed by L_{die} of zero and different R and $L_{mandrel}$. As can be seen, the amount of damage accumulated in the steady-state deformed region of tube extensively decreases by increase of $L_{mandrel}$. In addition, there is a critical $L_{mandrel}$ for each curvature radius in which the accumulated damage extensively falls. For example, when curvature radius of 2.5 mm is used, the accumulated damage in steady-state deformed region falls after the increase of $L_{mandrel}$ to 1.9 mm. Reasonably, this critical $L_{mandrel}$ can be selected as the minimum of this parameter in design of die/mandrel set. It is also notable that increase of $L_{mandrel}$ causes more contact between tube and die/mandrel surfaces which is discussed later. Therefore, more resistant frictional force occurs between these surfaces. This causes increase of hydrostatic pressure on tube wall which decreases the imposed damage through TCP. Besides this, the overall accumulated damage on tube generally decreases by increase of R as shown in Fig. 7. Despite this, the maximum imposed damage may increase by increase of R. For instance, when $L_{mandrel}$ of 0 mm is used, the maximum accumulated damage remarkably increases by increase of R from 2.5 to 5 mm. Since the maximum accumulated damage must be considered as the criterion for rupture prediction, the effect of R and $L_{mandrel}$ on this parameter is discussed later.

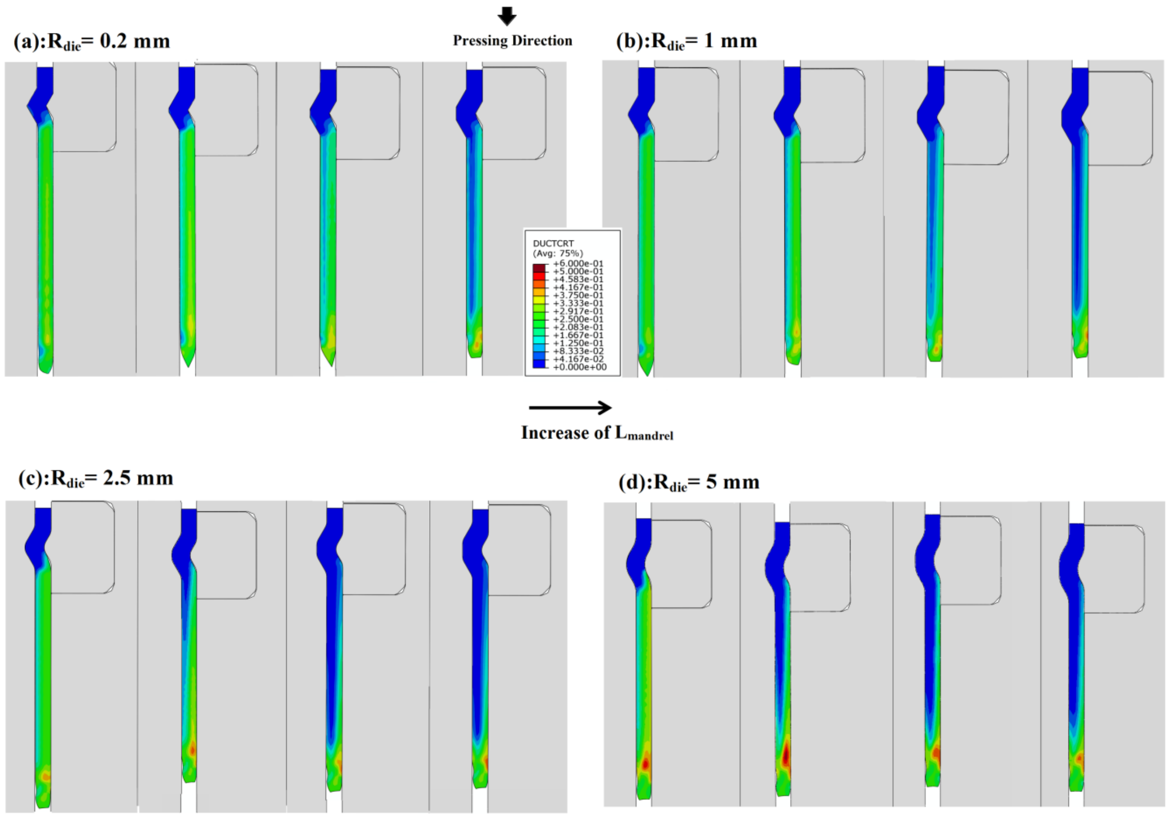

Fig. 7. The effect of $L_{mandrel}$ on accumulation of damage through TCP using L_{die} of zero and curvature radius (R) of: (a) 0.2 mm, (b) 1 mm (c) 2.5 mm and (d) 5 mm.

As shown in Fig. 8a to d, the decrease of R increases the imposed plastic strain. In addition, the increase of R generally increases the heterogeneity of imposed strain. However, this general trend has some exceptions. As an illustration, when $L_{mandrel}$ of 0 mm is used for die/mandrel set design, the heterogeneity of imposed strain decreases by increase of R from 0.2 to 1 mm. Besides this, it is notable that applying of small $L_{mandrel}$ combined with small R for TCP may result in deviated shapes of tube after the process. For example, the thinning and earing of tube wall may occur through processing by die/mandrel sets designed using small $L_{mandrel}$ combined with small R as shown in Fig. 8a and b. These deviated shapes of TCP processed tubes consequences experimental difficulties in further passes of the process and therefore, these designs cannot be considered as approvable. As shown in Fig. 9, when small $L_{mandrel}$ combined with small R are used, the distance between consequent shear stages of tube wall during the process is very low which results in incorrect route of tube wall through the bottleneck zone and therefore, increases strain heterogeneity and deviates shape of TCP processed tube. It is also notable that the bottleneck zone is filled more completely by tube wall when $R/L_{mandrel}$ increases since the greater $R/L_{mandrel}$ allows tube wall to manipulate its path due to longer distance between shear stages of TCP. This causes more long frictional contacts between die/mandrel and tube surfaces which decrease the imposed damage as mentioned previously. Besides this, increase of $L_{mandrel}$ decreases the heterogeneity of strain when R=0.2-2.5 mm are used as can be seen in Fig. 8 attributed to increase of distance between shear stages of TCP. Despite this, the heterogeneity of strain increases by the increase of $L_{mandrel}$ when R=5 mm is used which implies that the distance between shear stages of TCP has crossed its optimum amount.

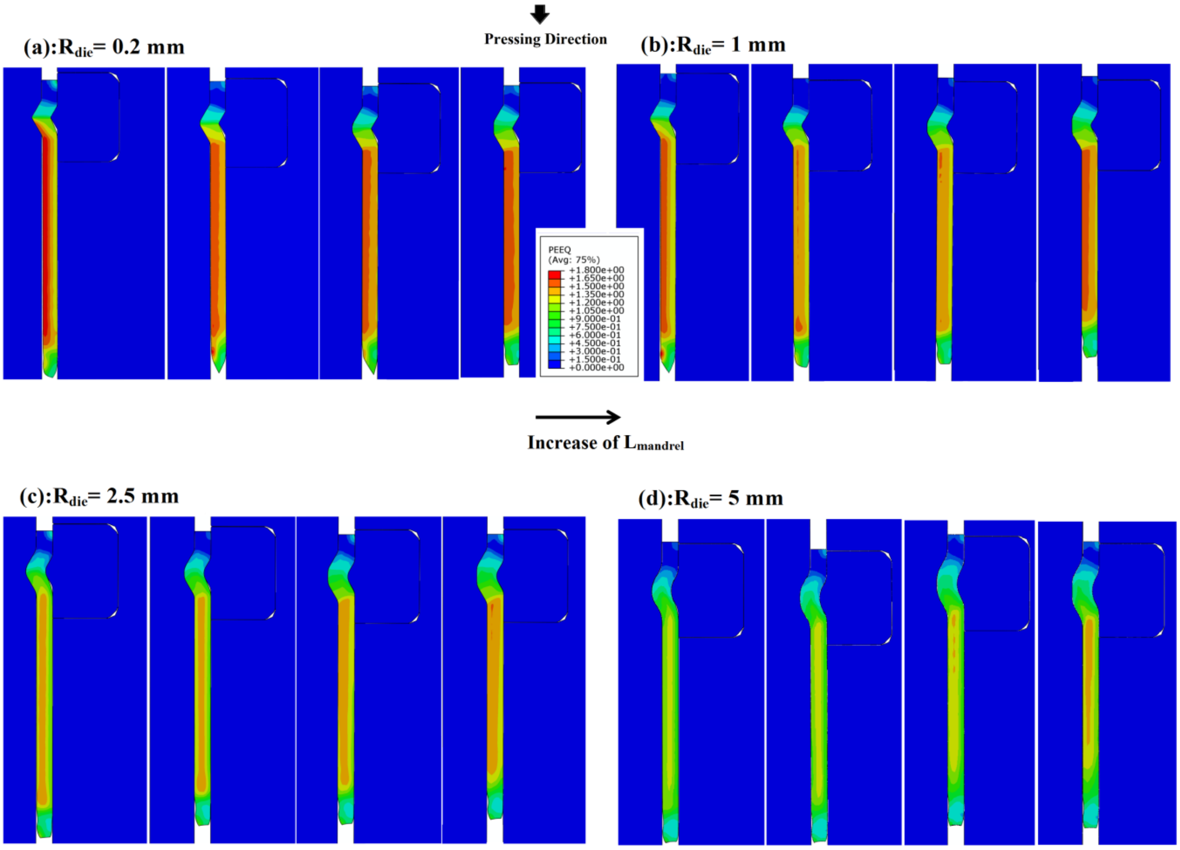

Fig. 8. The effect of $L_{mandrel}$ on distribution of plastic strain through TCP using L_{die} of zero and curvature radius (R) of: (a) 0.2 mm, (b) 1 mm (c) 2.5 mm and (d) 5 mm.

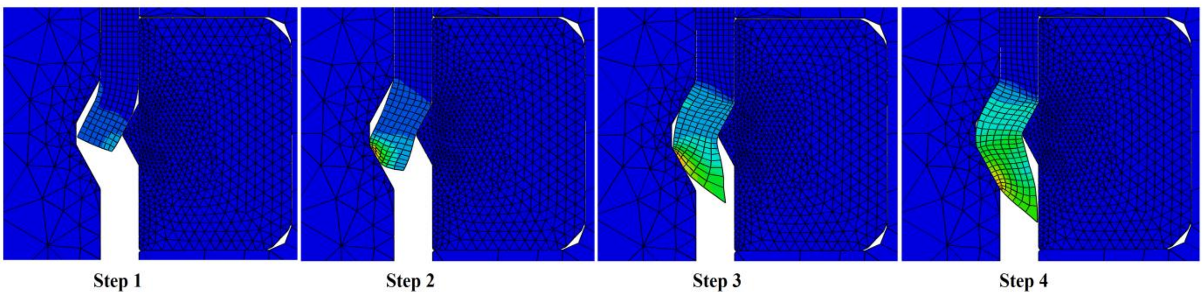

Fig. 9. Deformation steps of tube in a die/mandrel designed using L_{die} of 0 mm, $L_{mandrel}$ of 0.9 mm and curvature radius (R) of 0.2 mm.

Figure 10a compares the effect of R and $L_{mandrel}$ on the Average imposed Plastic Strain (APS) of the steady-state deformed regions of tubes processed by different die/mandrel sets of TCP designed by L_{die} of zero. Considering the hoop strains and the shear strains imposed by TCP [4, 8-9], the APS for each pass of TCP can be analytically calculated as:

$$Theoritical\ APS = 1.15\ \{4Cot\left(\frac{\Theta_{\text{channel}}}{2}\right) + 2Ln\left(\frac{\bar{D}_{tube}}{\bar{D}_{bottleneck}}\right)\} \tag{9}$$

where $\bar{D}_{tube}$ and $\bar{D}_{bottleneck}$ are the average diameters of tube before process and in the middle of bottleneck zone, respectively. Considering $\Theta_{channel}$, $\bar{D}_{tube}$ and $\bar{D}_{bottleneck}$ respectively equal to 150°, 22.5 mm and 18.8 mm, the APS is calculated as 1.65. This is relatively greater than the results of simulations since the theory considers imposed strain through a corner sharpen die (R of 0 mm) [4] while the used TCP dies/mandrels have relatively smooth corners. Note that the APS decreases by increase of R due to change of deformation mode of TCP from pure shear to shear combined with bending similar to the behavior reported for simple ECAP [15].

Figure 10b compares the effect of R and $L_{mandrel}$ on the Standard Deviation of plastic strain distribution per unit of average Plastic Strain (SDPS) through the steady-state deformed regions of tubes processed by different die/mandrel sets of TCP designed by L_{die} of zero. The SDPS of specimens processed by TCP are calculated as below:

$$SDPS = \frac{\sqrt{\frac{\sum_{i=1}^{n}(\varepsilon_i - APS)^2}{n}}}{APS} \tag{10}$$

where n is the number of nodes in tube thickness and ε_i is the imposed strain in each node. Note that the nodes placed on boundary of tube are considered with coefficient of 0.5 in calculation of APS and SDPS. As can be seen in Fig. 10b, when R=0.2-2.5 mm is used for TCP die/mandrel set, the SDPS decreases by increase of $L_{mandrel}$ up to 1.9 mm while more increase of $L_{mandrel}$ has a negligible effect on SDPS. This is more remarkable when R=0.2 mm is applied for designing TCP die/mandrel set whereas SDPS extensively falls after the increase of $L_{mandrel}$ from 0 mm. Despite this, for the designed die/mandrel sets using R=5-7.5 mm, the SDPS slightly increases by the increase of $L_{mandrel}$. In addition, the SDPS generally increases by the increase of R, although this has few exceptions. For instance, the increase of R between 0.2 to 2.5 mm has negligible effect on SDPS when $L_{mandrel}$ of 1.9 mm is selected. Moreover, the SDPS falls by increase of R from 0.2 mm when $L_{mandrel}$ of 0 mm is selected. These effects are due to incorrect path of tube wall through bottleneck region of TCP for die/mandrel sets designed by both small R and small $L_{mandrel}$ mentioned before. Comparing these results, one can presume that if proper $L_{mandrel}$ and R are selected, the SDPS can be remarkably diminished.

Figure 10c compares the effect of R and $L_{mandrel}$ on Maximum accumulated Damage per unit of average Plastic Strain (MDPS) through the steady-state deformed regions of tubes processed by different die/mandrel sets of TCP designed by L_{die} of zero. As can be seen, the MDPS extensively falls by the increase of $L_{mandrel}$ when R=5-7.5 mm is used. However, when R=0.2-2.5 mm is used, the MDPS only falls when $L_{mandrel}$ reaches to 1.9 mm. In addition, although the increase of R generally increases MDPS, the variation of MDPS by the increase of R from 0.2 mm up to 5 mm is negligible when the $L_{mandrel}$ is equal or greater than 1.9 mm. Considering explanation of Fig. 10c, it can be established that MDPS is impressively lowered by selection of $L_{mandrel}$ about or greater than 1.9 mm and R=0.2-5 mm.

Considering explanations of Fig. 10, it can be demonstrated that the new geometry of TCP imposes more intense strain, results in less strain heterogeneity and causes lower risk of rupture in comparison of the conventional geometry. As an illustration, the APS of new geometry of TCP is 20-50% higher than the conventional one’s while the SDPS and MDPS can be a few times less than the conventional one’s. In addition, the new geometry of TCP is optimized using proper amounts for L_{die}, $L_{mandrel}$ and R. For instance, the optimum amounts for L_{die} is 0 mm since increase of this parameter increases the strain heterogeneity, rupture risk and waste of tube. In addition, the optimum amount of $L_{mandrel}$ is about 2-3 mm in order to decrease strain heterogeneity and rupture risk of tube through TCP. As can be seen, the optimum $L_{mandrel}$ is very close to the second scenario of mandrel design presented in Eq. (4) and line 2 of Fig. 2 (b). Moreover, to prevent deviated shapes of tube besides the decrease strain heterogeneity and rupture risk through TCP, the amount of R for used TCP die/mandrel sets shall be selected about 1-2.5 mm which is 0.3-0.7 time of tube thickness.

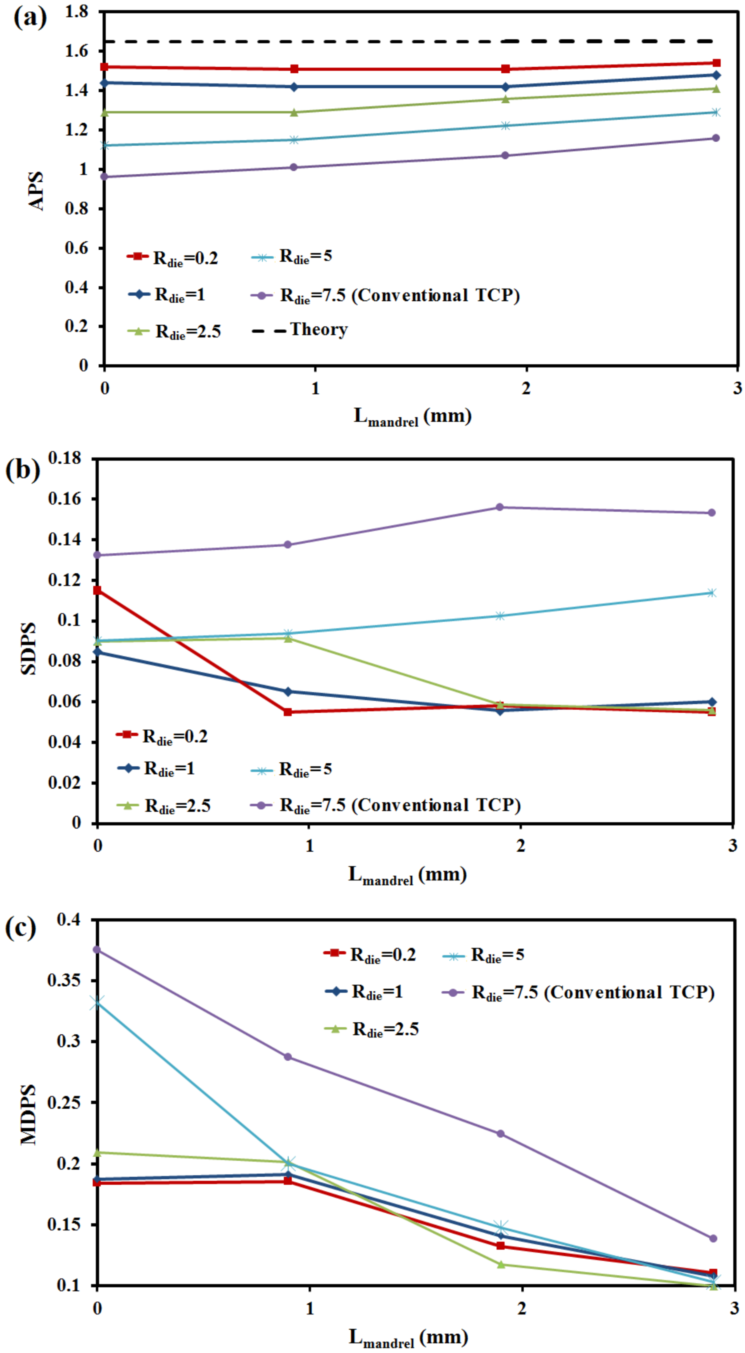

Fig. 10. Comparison of effects of $L_{mandrel}$ and curvature radius (R) on the: (a) Average imposed Plastic Strain (APS), (b) Standard Deviation of strain distribution per unit of average Plastic Strain (SDPS) and (c) Maximum Damage per unit of average Plastic Strain (MDPS) for steady-state deformed regions of tubes processed by different die/mandrel sets of TCP designed by L_{die} of zero.

5. Conclusion

Considering results of this work, it can be concluded that:

1- The applied simulation method complemented by a proper damage criterion can predict the rupture of aluminum 6061-O alloy tube subjected to TCP process.
2- Using the applied simulation method, a new geometry for TCP process is examined which causes less strain heterogeneity, less risk of rupture and more intense plastic strain.
3- The optimum amount of L_{die} for this new geometry of TCP is 0 mm which decreases the accumulated damage, strain heterogeneity and waste of the tube during the process.
4- The optimum amount of $L_{mandrel}$ for new geometry of TCP is obtained by considering the geometry of conventional ECAP at second shear stage of TCP as presented in the second line of Fig. 2 (b) and Eq (4).
5- To prevent deviance of processed tube shape and to obtain less strain heterogeneity combined with less damage per unit of plastic strain, a relatively smooth die/mandrel shall be designed for TCP using a curvature radius about 0.3-0.7 time of tube thickness.

Acknowledgements: The author wishes to thank the research board of Ferdowsi University of Mashhad (FUM) for the financial support and the provision of research facilities used in this work through the project number of 2/37062.

6. References

[1] V. M. Segal, Material processing by simple shear, *Mater Sci Eng*, 197A (1995) 157–64.
[2] R. Z., Valiev, N. A. Krasilnikov and N. K., Tsenev, Plastic deformation of alloys with submicron-grained structure, *Mater Sci Eng A,* 137 (1991) 35-40.
[3] N. Tsuji, Y., Saito, H., Utsunomiya and S. Tanigawa, Ultrafine grained bulk steel produced by Accumulative Roll-Bonding (ARB) process, *Scr Mater,* 40 (1999) 795–800.
[4] Y. Estrin and A. Vinogradov, Extreme grain refinement by severe plastic deformation: A wealth of challenging science, *Acta Mater*, 61 (2013) 782–817.
[5] M. S. Mohebbi, and A. Akbarzadeh, Accumulative spin bonding (ASB) as a novel SPD process for fabrication of nanostructured tubes, *Mater Sci Eng A*, 528 (2010) 180–8.
[6] L. S. Toth, M. Arzaghi, J. J. Fundenberger, B. Beausir, O. Bouaziz and R. A. Massion. Severe plastic deformation of metals by high-pressure tube twisting, *Scr Mater,* 60 (2009) 175–7.
[7] A. V. Nagasekhar, U. Chakkingal and P. Venugopal, Candidature of equal channel angular pressing for processing of tubular commercial purity-titanium, *J Mater Proc Tech*, 173 (2006) 53–60.
[8] A. Zangiabadi and M. Kazeminezhad. Development of a novel severe plastic deformation method for tubular materials: Tube Channel Pressing (TCP), *Mater Sci Eng A*, 528 (2011) 5066-72.
[9] M. H. Farshidi and M. Kazeminezhad, The effects of die geometry in tube channel pressing: Severe plastic deformation. J Mater Design App: In press: http://dx.doi.org/10.1177/1464420715569289.
[10] G. Faraji, M. M. Mashhadi, A. F. Dizadji, and M. Hamdi, A numerical and experimental study on tubular channel angular pressing (TCAP) process. *J Mech Sci Tech*, 26 (2012) 3463-8.
[11] V. Tavakkoli, M. Afrasiabi, G. Faraji and M. M. Mashhadi, Severe mechanical anisotropy of high-strength ultrafine grained Cu–Zn tubes processed by parallel tubular channel angular pressing (PTCAP), *Mater Sci Eng A*, 625 (2015) 50–5.
[12] M. H. Farshidi and M. Kazeminezhad, Deformation behavior of 6061 aluminum alloy through tube channel pressing: Severe plastic deformation, *J Mater Eng Perform,* 21 (2012) 2099–105.
[13] G. Faraji, M. M. Mashhadi and H. S. Kim, Deformation behavior in Tubular Channel Angular Pressing (TCAP) using triangular and semicircular channels, *Mater Transact*, 53 (2012) 8-12.

[14] N. Medeiros, L. P. Moreira, J. D. Bressan, J. F. C. Lins and J. P. Gouvea, Upper-bound sensitivity analysis of the ECAE process, *Mater Sci Eng A*, 527 (2010) 2831–44.

[15] C. J. Luis Perez, On the correct selection of the channel die in ECAP processes, *Scr Mater*, 50 (2004) 387–93.

[16] A. P. Zhilyaev, K. Oh-ishi, G. I. Raab and T.R. McNelley, Influence of ECAP processing parameters on texture and microstructure of commercially pure aluminum, *Mater Sci Eng A*, 441 (2006) 245–52.

[17] M. H. Farshidi, M. Kazeminezhad and H. Miyamoto, Microstructrual evolution of aluminum 6061 alloy through Tube Channel Pressing, *Mater Sci Eng*, 615 *A* (2014) 139-47.

[18] V. Patil Basavaraj, U. Chakkingal and T. S. Prasanna Kumar, Effect of geometric parameters on strain, strain inhomogeneity and peak pressure in equal channel angular pressing – A study based on 3D finite element analysis, *J Manuf Proc*, 17 (2015) 88–97.

[19] R. Luri, C. J. Luis Perez, D. Salcedo, I. Puertas, J. Leon, I. Perez J. P. Fuertes. Evolution of damage in AA-5083 processed by equal channel angular extrusion using different die geometries, *J Mater Proc Tech*, 211 (2011) 48–56.

[20] S. Li, M.A.M. Bourke, I.J. Beyerlein, D. J. Alexander and B. Clausen, Finite element analysis of the plastic deformation zone and working load in equal channel angular extrusion, *Mater Sci Eng*, 382A (2004), 217–36.

[21] M. Kazeminezhad and E. Hosseini, Modeling of induced empirical constitutive relations on materials with FCC, BCC, and HCP crystalline structures: severe plastic deformation, *Int J Adv Manuf Tech*, 47 (2010) 1033–9.

[22] A. Kacem, A. Krichen, P. Y. Manach, S. Thuillier and J. W. Yoon, Failure prediction in the hole-flanging process of aluminium alloys. *Eng Fract Mech*, 99 (2013) 251–65.

[23] Y. Bao and T. Wierzbicki, On fracture locus in the equivalent strain and stress triaxiality space, *Int J Mech Sci*, 46 (2004) 81–98.

[24] H. L. Yu and D. Y. Jeong, Application of a stress triaxiality dependent fracture criterion in the finite element analysis of unnotched Charpy specimens, *Theo App Fract Mech*, 54 (2010) 54–62.

هندسه‌ای جدید برای فرآیند فشار در کانال لوله‌ای: تغییر شکل مومسان شدید لوله

محمد حسن فرشیدی

گروه مهندسی متالورژی و مواد، دانشکده مهندسی دانشگاه فردوسی مشهد، مشهد، ایران

چکیده : بدلیل آنکه لوله‌ها کاربردهای صنعتی گوناگونی دارند، اعمال تغییر شکل مومسان شدید بر روی آن‌ها هدف بسیاری از پژوهش‌ها بوده است. از این میان، توسعه فرآیندهای تغییر شکل مومسان شدید لوله‌ها بر مبنای فرآیند" فشار در کانال زاویه‌دار همسان[1]"، موفق‌تر بوده است. به عنوان نمونه، فرآیند "فشار در کانال لوله‌ای[2]" به عنوان یک فرآیند قابل توجه برای تغییر شکل مومسان شدید لوله‌ها مطرح شده است چراکه می‌تواند برای ابعاد گوناگون لوله‌ها مورد استفاده قرار گیرد. با این‌حال، از آن‌جا که هندسه قالب و ماندرل بر رفتار تغییر شکل لوله در این فرآیند اثر چشمگیری دارند، پژوهش‌های بیشتری باید بر روی بهینه‌سازی هندسه این اجزاء صورت پذیرد. این پژوهش به منظور آزمودن هندسه جدیدی برای فرآیند فشار در کانال لوله‌ای به منظور کاهش ناهمگنی کرنش اعمالی و خطر گسیختگی لوله در این فرآیند، انجام شده است. بدین منظور، اثر متغیرهای هندسی مختلف بر رفتار تغییر شکل لوله در این فرآیند به روش اجزا محدود شبیه سازی شد. در این شبیه سازی، خطر گسیختگی لوله از طریق یک تابع آسیب ارزیابی گردید و سپس نتایج شبیه سازی با آزمون‌های عملی مقایسه گردید. نتایج نشان داد که هندسه جدید فرآیند، سبب افزایش کرنش اعمالی و کاهش ناهمگنی کرنش و خطر گسیختگی لوله در فرآیند می‌شود. به علاوه، مقایسه نتایج آزمون‌های عملی با شبیه سازی‌ها نشان داد که روش شبیه سازی بکار برده شده، به خوبی می‌تواند گسیختگی لوله حین فرآیند را پیش بینی نماید. همچنین، میزان بهینه متغیرهای هندسی فرآیند از طریق شبیه سازی محاسبه گردید.

کلمات کلیدی: تغییر شکل مومسان شدید، لوله، شبیه سازی به روش اجزای محدود، توزیع کرنش، پیش‌بینی گسیختگی

---
[1] Equal Channel Angular Pressing (ECAP)
[2] Tube Channel Pressing (TCP)